Numerical simulation of flashing jets atomisation using a unified approach

Konstantinos G. Lyras[a], Siaka Dembele[a], Jennifer X. Wen[b,*]

[a] *Department of Mechanical and Automotive Engineering, Kingston University London, SW15 3DW, London, UK*
[b] *School of Engineering, University of Warwick, Coventry, UK*

Abstract

The physics of the atomisation of flash boiling jets is known to be extremely complex with interactions of different mechanisms at microscopic and macroscopic level. Early studies describe both the mechanical and thermodynamic effects focusing on the influence of the initial pressure and temperature on the spray characteristics. The resulting flashing jet usually emerges to the low-pressure region with a high velocity and fragments to large blobs and ligaments which break up to droplets due to both mechanical and thermodynamic effects. This present study describes a numerical approach for simulating the atomisation of flashing liquids suitable for both primary atomisation and secondary break-up using the Eulerian-Lagrangian-Spray-Atomisation model coupled with a pressure equation for the metastable jet. The proposed approach aims at describing the atomisation of superheated jets and the impact of bubble nucleation at different stages and regimes inside the channel the liquid emerges from. The changes in the regime outside the nozzle are discussed for various cases of flashing liquids providing insights for the interactions of the mechanisms that contribute to the liquid fragmentation and the spray characteristics such as the droplet size and velocity and the spray angle.

Keywords: flashing, boiling, atomisation, ELSA model

*Corresponding author
Email address: jennifer.wen@warwick.ac.uk (Jennifer X. Wen)

1. Introduction

The disintegration of liquid jets from a higher pressure region to a lower pressure environment is a process where multiple interactions take place. Depending on the application a pressure drop may occur when the liquid flows through a nozzle or a pipe. If the pressure drops below the vapour pressure, a rapid phase change begins which is generally termed flashing. In case of pure cavitation, the pressure recovers above the limit of the vapour pressure unlike the extreme case of flashing in which pressure remains below the saturation pressure. Both of these processes have multiple industrial applications in fuel spray injection systems, health and safety in nuclear energy and in aerosol industries to name a few. Prior research studies from Oza (1984) and Ishii (1975) suggest that flash boiling is associated to three different processes, which are, bubble nucleation, bubble growth and atomisation. In order to establish a modelling strategy for flashing one has to give an illustration of the factors that contribute to this multi-facet problem. Flashing of a liquid can occur when the fluid, initially being either sub-cooled or saturated, follows an isothermal pressure drop or an isobaric heating path respectively. As long as the liquid moves towards the low pressure region, the pressure drops and upon reaching the liquid saturation curve it becomes superheated yielding a wide range of droplet sizes stemming from an explosive atomisation at the exit of the channel. In cases of a liquid flowing within a channel, the fluid might be superheated inside or outside the channel depending on the geometry and the thermodynamic conditions.

Experimental investigations on the nucleation kinetics report a different response of the liquids in the temperature variations which corresponds to different nucleation rates (Pavlov, 1988). The intensity of the bubble nucleation rate generally leads to an enhanced boiling and is a primary cause of change in the flow regime which might be combined with a shattering of the jet attributing explosive characteristics to the process. Previous studies have shown that even small changes in temperature may alter the jet structure (Park and Lee, 1994). In light of this, it is likely to have a two-phase jet inside the nozzle with a variety of

possible regimes (Sher et al., 2008; Park and Lee, 1994). A paradigm of the most crucial parameters for bubble nucleation is the geometry of the nozzle the fluid flows through (Park et al., 1997). Many studies have been carried out regarding the expected regimes in industrial depressurisations applications (van den Bosch and Waterings, 2005; Benajes et al., 2004; Yildiz, 2005; Cleary, 2008). Usually, phenomenological approaches induced from experiments consider the length-to-diameter of the nozzle to be the integral geometrical parameter that influences the flow regime. The resulting jet can be thought as the outcome of two mechanisms; the fluid instabilities (i.e. Kelvin-Helmholtz) and the boiling conditions together with bubble nucleation. These mechanisms act within the jet in a competing way and give rise to a violent disintegration, characteristic of the flashing process. Flashing continues until the generated vapour has enough energy to achieve equilibrium. Thermodynamic and mechanical effects act inside the jet and on the jet surface altering the jet shape and dynamics. The pressure drops rapidly leading to a phase transition in cases of cavitation and flashing. During flashing bubbles form and grow from the vapour clusters. The changes that happen in a microscopic level vary locally in time and space and is hard to define a characteristic spatial scale for the liquid structures. The liquid break-up gives droplets with a spectrum of sizes from a droplet size (d_{max}) of the order of some millimetres to a minimum size which can be thousands of times less.

Various experimental works have been conducted in the last three decades for unravelling the mysteries of the liquid atomisation of flashing jets. Reitz (1990) studied flash boiling atomisation of water under relatively small pressure (p_{inj}) and different initial temperatures (T_{inj}). The jet was well atomised giving small sized droplets that dispersed downstream the nozzle exit. The majority of the droplet sizes was measured to be around $100\mu m$. The flow was bubbly with a two-phase jet observed outside the nozzle with minimum and maximum droplet diameters varying around two orders of magnitude. The droplet diameter decreased along the radial direction by contrast to the trend at the axial direction. Similar scales for the drop diameter were reported by Allen (1998) for

flashing propane jets. The diameters measured, were within the range of some microns up to $500\mu m$ for a storage pressure of 6 bar. Some insights for the velocity profiles across the jet were obtained. The velocity had a characteristic bell shape with a maximum at the jet centreline. The velocity decreased moving further away the nozzle exit while preserving the same shape. The change in the regime of the jet was observed. The change in the measured drop sizes was attributed to the bubbles that burst each other giving new drops with smaller diameter. Park and Lee (1994) using flashing water provided some interesting details regarding the anatomy of flashing jets. The droplet sizes were measured at various locations at the radial direction. The higher size at the jet centreline indicated an intact liquid core which progressively disintegrated across the radial and axial directions. Similar velocity profiles at different locations are also reported in the literature in the work of Yildiz (2005) for flashing R134A jets with high degrees of superheat. Although the velocities at the radial direction of flashing jets tend to follow the same trend as non-flashing jets (as illustrated in (Abramovich, 1963), the axial behaviour of velocity is expected to change regarding if flashing happens inside or outside the nozzle.Hervieu and Veneau (1996) provided some results for the jet shape of flashing jets for propane releases but did not include details for the spray angles. Park and Lee (1994) illustrated the spray angle and how it changes with respect to the initial flow conditions. They showed that the spray angle increased while increasing the initial temperature with values smaller to 90^oC. Recently, Wang et al. (2017) studied the effect of the internal flow patterns in the spray dynamics. In their study for flashing R134A jets the flow was bubbly for relatively small storage pressure ($p \leq 15bar$) with nucleation occurring at random locations and the spray angle increasing for higher pressure.

Empirical models for the spray properties of superheated consider the geometry and initial conditions jets in a zero-dimensional correlations (Johnson and Woodward, 1999; van den Bosch and Waterings, 2005; Witlox and Bowen, 2002). A common practice to tackle the varying thermodynamic effects which play a major role in the emerging jet is the use of reasonable assumptions for

the release process. The isenthalpic and isentropic assumptions are possible for the expansion region of the flashing jets. In the isenthalpic formulations the change in the kinetic energy is small compared with the enthalpy change. On the other hand, in case of isentropic conditions either the momentum equation is replaced with an entropy equation or the energy equation is substituted in favour of well-established isentropic relationships. The shortcomings of the isenthalpic and isentropic assumptions are not apparent and there is an ambiguity in the literature regarding the assumption to be made for flashing expansion.

The most recent state of the art three-dimensional CFD studies for flashing, including the Homogeneous Relaxation Model (HRM), are implemented following Schmidt et al. (2010). Moulai et al. (2015) and Duke et al. (2015) used HRM and successfully calculated the mass flow rate and the liquid penetration. Price et al. (2016) used an evaporation model for simulating flashing jets using Lagrangian particle tracking with the droplet shape changing due to flashing providing validation for the liquid penetration. Characterisation of the spatial scale of the liquid blobs and ligaments is still an ongoing research topic and poses significant challenges due to the multi-scale nature of the process.

The complex interactions during the atomisation of superheated jets pose the biggest challenge for three-dimensional CFD models for calculating the size and velocity of the droplets. One of the major difficulties for modelling the atomisation of superheated jets regarding physics is the metastable two-phase mixture that occurs during depressurisation. This paper presents a numerical approach for simulating the atomisation of flashing liquids accounting for the distinct stages, from primary atomisation to secondary break-up to small droplets using the Eulerian-Lagrangian-Spray-Atomisation model coupled with the HRM. The Σ-equation is implemented and solved in a fully Eulerian approach for tracking liquid structures of any shape, and computes the spray characteristics. A modified version for the transport equation of the surface density is used and a new source term accounting for the changes in Σ due to evaporation in both dense and dilute spray regions is added. The HRM is a reliable model accounting for the non-equilibrium vapour generation and can

be easily implemented in an Eulerian framework taking advantage of the more detailed representation of the primary atomisation region in such approaches. An algorithm that links the standard pressure-velocity coupling algorithm to the HRM and volume of fluid method is used as a basis to simulate cryogenic and water jets (Lyras et al., 2018). The method has been previously derived for examining the internal flow regimes of superheated liquids and is coupled here with a spray model for modelling atomisation.

The proposed approach has the advantage of avoiding the unrealistic common assumption of pure liquid rather than a mixture at the nozzle exit. It models the change in the regime inside the nozzle treating flashing in a unified approach simulating the metastable jet both inside and outside the nozzle. Important mechanisms such as thermal non-equilibrium, aerodynamic break-up, droplet collisions and evaporation are modelled in a novel atomisation model. Results for turbulent flows for superheated liquids are presented showing that the proposed approach can accurately simulate the primary atomisation.

2. Numerical modelling of flash boiling

2.1. Non-equilibrium vapour generation

The vapour mass fraction (denoted as x hereafter) is calculated for both the internal flow and atomisation region. Introducing the transport equation in a compressible framework with a mixture density ρ and a velocity field u_j it is given as,

$$\frac{\partial \rho x}{\partial t} + \frac{\partial \rho u_j x}{\partial x_j} = \Gamma \tag{1}$$

The term Γ stands for the vapour generation rate. Vapour mass fraction is changing through time and space and needs to be modelled for closure. Following Downar-Zapolski et al. (1996) as first approximation, x can be assumed to relax towards an equilibrium value, x_{eq} at a time-scale Θ that is locally

dependent on pressure. The HRM is written in the following way,

$$\Gamma = -\rho \left(\frac{x - x_{eq}}{\Theta} \right) \tag{2}$$

This is first order approximation to Γ using Taylor series expansion. This formulation attains an exponential tendency for the system from an initial state x_0 to equilibrium through time,

$$x = x_{eq}(1 - e^{-\frac{t}{\Theta}}) + x_0 e^{-\frac{t}{\Theta}} \tag{3}$$

The equilibrium value for the vapour mass fraction can be calculated as,

$$x_{eq} = \frac{h - h_{l,sat}}{h_{v,sat} - h_{l,sat}} \tag{4}$$

In this formulation, $h_{l,sat}, h_{v,sat}$ are the saturated enthalpies of liquid and vapour state. The timescale for the model is calculated as,

$$\Theta = \Theta_0 \alpha^{-0.257} \psi^{-2.24} \tag{5}$$

The non-dimensional pressure ψ is equal $(p_{sat} - p)/p_{sat}$. The timescale Θ is a function of the constant $\Theta_0 = 6.51 \times 10^{-4}[s]$ and local densities. The void fraction is calculated from the liquid and vapour densities ρ_l, ρ_v as $\alpha = (\rho_l - \rho)/(\rho_l - \rho_v)$. The last two equations have been derived from Downar-Zapolski et al. (1996) for water jets at initial pressure up to $100kPa$. The low-pressure correlation for HRM has been used before for superheated R134A Lyras et al. (2017).

2.2. Pressure calculation

The concept of the pressure equation is to create an equation that encapsulates all the processes involved in the fluid flow motion. The algorithm of Lee et al. (2009) and Schmidt et al. (2010) has been used as a basis. Since density is a function of pressure, temperature and quality, $\rho = \rho(p, h, x)$. Following Bilicki and Kestin (1990), the material derivative of density becomes

$$\frac{D\rho}{Dt} = \left(\frac{\partial \rho}{\partial p} \right)_{h,x} \frac{Dp}{Dt} + \left(\frac{\partial \rho}{\partial h} \right)_{p,x} \frac{Dh}{Dt} + \left(\frac{\partial \rho}{\partial x} \right)_{p,h} \frac{Dx}{Dt} \tag{6}$$

Combining with the continuity equation

$$-\rho\frac{\partial u_i}{\partial x_i} = \left(\frac{\partial \rho}{\partial p}\right)_{h,x}\frac{Dp}{Dt} + \left(\frac{\partial \rho}{\partial h}\right)_{p,x}\frac{Dh}{Dt} + \left(\frac{\partial \rho}{\partial x}\right)_{p,h}\frac{Dx}{Dt} \tag{7}$$

The momentum equation in a matrix notation following Jasak (1996) is

$$a_P u_P = H(u_j) - \frac{\partial p}{\partial x_i} + F_\sigma \tag{8}$$

In this formulation, a_P is the diagonal coefficients tensor for a cell P and $H(u_j)$ is the coefficient matrix for all the neighbours of P including other source terms except for the pressure gradient. Solving for u_P (denoted with u hereafter) and substituting to Eq.(7) a matrix equation for pressure is obtained

$$\begin{aligned}&\rho\frac{\partial}{\partial x_j}\left(\frac{1}{a_p}H(u_j)\right)_f - \rho\frac{\partial}{\partial x_j}\left(\frac{1}{a_p}\frac{\partial p}{\partial x_i}\right) + \rho\frac{\partial}{\partial x_j}\left(\frac{1}{a_p}F_\sigma\right) + \left(\frac{\partial \rho}{\partial p}\right)_{h,x}\frac{Dp}{Dt}\\ &+ \left(\frac{\partial \rho}{\partial h}\right)_{p,x}\frac{Dh}{Dt} + \left(\frac{\partial \rho}{\partial x}\right)_{p,h}\frac{Dx}{Dt} = 0\end{aligned} \tag{9}$$

The operator $()_f$ stands for the interpolation to the cell faces. In cases of air entrainment to the mixture another term can be added to this last equation. Introducing an indicator function γ for the mixture (liquid and its vapour) ($\gamma = 1$ for no air and $\gamma = 0$ in case of no mixture) and substituting the HRM expression the pressure equation becomes

$$\begin{aligned}&\rho\frac{\partial}{\partial x_j}\left(\frac{1}{a_p}H(u_j)\right)_f - \rho\frac{\partial}{\partial x_j}\left(\frac{1}{a_p}\frac{\partial p}{\partial x_i}\right) + \rho\frac{\partial}{\partial x_j}\left(\frac{1}{a_p}F_\sigma\right)\\ &+ \left(\frac{\partial \rho}{\partial p}\right)_{h,x}\frac{Dp}{Dt} + \left(\frac{\partial \rho}{\partial h}\right)_{p,x}\frac{Dh}{Dt} + \left(\frac{\partial \rho}{\partial x}\right)_{p,h}\left(\frac{x - x_{eq}}{\Theta}\right) + \left(\frac{\partial \rho}{\partial \gamma}\right)\frac{D\gamma}{Dt} = 0\end{aligned} \tag{10}$$

This equation is used for the pressure update (without the pressure gradient correction) and includes the effects of the surface tension, thermal non-equilibrium and multiphase mixing (Lyras et al. 2018). In this paper an additional term for thermal expansion is incorporated. The densities of each phase k with compressibility Ψ_k are calculated using a linear approximation from a reference state (saturation conditions) of the following form

$$\rho_k = \rho_{ref} + \Psi_k(p - p_{ref}) \tag{11}$$

The rest of the mixture properties are calculated as in Lyras et al. (2018).

2.3. Interface tracking

The volume of fluid (VOF) approach is used here to capture the interface between the liquid and gaseous phases. VOF method is a distinct interface capturing method for resolving the inter-phase dynamics (Prosperetti and Tryggvason, 2009). Surface forces due to liquid-gas interfacial instabilities can be significant for the spray dynamics (Crowe, 2005). VOF has been employed before for cavitating flows by Ishimoto et al. (2008), Edelbauer (2017) and Srinivasan et al. (2010) and for non-evaporating sprays by Tomar et al. (2010) and Ling et al. (2015). In cases of mass transfer due to phase change, the interface changes through time and space at any direction. This is included in the continuity equation and consequently in the pressure equation. The liquid mass fraction is updated first for the VOF term in the momentum equation in favour of the volume fraction which is generally recommended in incompressible flows (Jiang et al., 2010). The continuum surface force (CSF) of Brackbill et al. (1992) is used to calculate the surface tension force in the momentum equation. This force is acting on the liquid-gas interface and is explicitly calculated as

$$F_\sigma = \sigma \kappa \nabla \phi_l \tag{12}$$

The liquid volume fraction ϕ_l is calculated from the mass fraction of the liquid according to Lyras et al. (2018). The surface tension is denoted with σ and the curvature of the interface with κ and is given by

$$\kappa = -\nabla \cdot \left(\frac{\nabla \phi_l}{|\nabla \phi_l|} \right) \tag{13}$$

This expression is added to the pressure equation. The HRM and VOF are naturally coupled together addressing different inherent physical phenomena. This is a volume conservative formulation and is adopted for both the flow inside the channel and the primary and secondary break-up.

3. Liquid atomisation

The characterisation of liquid atomisation can be considered as a problem of describing the small liquid volumes of arbitrary shape in the three-dimensional

space. In two phase flows (liquid and gas) the two fluids are separated by an interface. The presented method in this paper considers liquid/gas cases, although the same method applies to two immiscible fluids e.g. two liquids (Lhuillier, 2003). The interface is a two-dimensional surface in the three-dimensional space. The representation in space $\mathbf{x} = (x, y, z)$ and time t of this surface S can be done through a geometrical constraint $F(\mathbf{x}, t) = 0$ (Aris, 1962). The phase indicator function can be defined via a Heaviside function $H()$ (Prosperetti and Tryggvason, 2009) as

$$\phi_l(\mathbf{x}) = 1 - \phi_g(\mathbf{x}) = H(F(\mathbf{x}), t) \tag{14}$$

For each phase k, liquid (l) or gas (g), $\phi_k = 1$ if and only if $\mathbf{x}$ lies inside phase k. The velocity at the surface S is then $u_c = (\partial \mathbf{x}/\partial t)_S$. Since the function F becomes zero at the interface, its material derivative is zero

$$\frac{\partial F}{\partial t} + u_c \cdot \frac{\partial F}{\partial x_j} = 0 \tag{15}$$

From the last two equations it is clear that every velocity field with the same normal component will produce the same same motion of the interface. Since the normal unit vectors are $n_l = -n_g = \nabla F/|\nabla F|$, this normal velocity is equal to $u_c \cdot n_l = -u_c \cdot n_g = \frac{(\partial F/\partial t)}{|\nabla F|}$. Recalling the definition of the phase indicator ϕ_k, for each phase k, $\nabla \phi_l = -\nabla \phi_g = \delta(F)\nabla F$ where $\delta()$ is the Dirac function. Now the local instantaneous interfacial area concentration (fine-grained surface density) δ_I can be defined as $\delta_I \equiv -n_k \cdot \nabla \phi_k = \delta(F)|\nabla F|$. This definition is employed from Marle (1982), Kataoka et al. (1986), Lhuillier (2003) and Morel (2007). Using the microscopic velocity u_c, Lhuillier (2003) has demonstrated an equation for the evolution of δ_I using the following transport equation

$$\frac{\partial \delta_I}{\delta t} + u_c \cdot \frac{\partial \delta_I}{\partial x_j} = -\delta_I n_i n_j : \frac{\partial u_c}{\partial x_j} \tag{16}$$

Following Ishii (1975) and Delhaye (1976) the ensemble average of δ_I is equal to the integral of the fine-grained surface density over a volume V with surface S which is equal to the surface density $\Sigma(\mathbf{x}, t) =< \delta_I >= \frac{1}{V}\int_V \delta_I \mathrm{d}V = \frac{S(\mathbf{x},t)}{V}$. In cases of zero mass flux at the interface (zero reaction rate) the velocity u_c

is equal to the fluid velocity u_j. Integration of Eq.16 over V and using the definition of Σ leads to an equation for the surface density

$$\frac{\partial \Sigma}{\partial t} + u_j \cdot \frac{\partial \Sigma}{\partial x_j} = -\Sigma n_i n_j : \frac{\partial u_i}{\partial x_j} \tag{17}$$

Because of the complex motion of the interface, the associated quantities responsible for the description of Σ such as the interfacial stress or the interfacial orientation tensors need to be averaged. Hence the average Σ in space is used hereafter.

3.1. An equation for surface density

The equation for the evolution of the surface density in time and space Eq.17, contains in the RHS all factors that cause changes in a macroscopic level. The surface can be produced and destroyed by different dynamic processes happening during the atomisation. Vallet and Borghi (1999) illustrated a model for the including the effect of these processes in Σ. This approach, the so-called $\Sigma - Y$ model was established in an Eulerian framework and gave rise to the Eulerian-Lagrangian-Spray-Atomisation (ELSA) method (Vallet et al., 2001). In this paper the model proposed by Menard et al. (2006) and modified by Lebas et al. (2009) is used as basis. The model defines different source terms which describe the surface change due to turbulence, aerodynamic break-up and evaporation. Here, the model is written splitting the evaporation term into a dense and dilute part $(S_{vap,den}, S_{vap,dil})$ as

$$\begin{aligned} &\frac{\partial \bar{\Sigma}}{\partial t} + \frac{\partial \tilde{u_j} \bar{\Sigma}}{\partial x_j} = \frac{\partial}{\partial x_j}\left(\frac{\nu_t}{Sc_t}\frac{\partial \bar{\Sigma}}{\partial x_j}\right) + \Psi\left(S_{init} + S_{turb} + S_{vap,den}\right) + \\ &\left(1 - \Psi\right)\left(S_{coll} + S_{2ndBU} + S_{vap,dil}\right) \end{aligned} \tag{18}$$

The Reynolds average, $\bar{\Sigma}$ is used and $\tilde{u_j}$ is the mass weighted Favre average of velocity. The model consists of several source terms on the RHS, which are associated with different processes that might have an impact on the atomisation. This approach extends the original model of Vallet and Borghi (1999) considering different and more mechanisms which can potentially alter the interface evolution. The source terms can be calculated via different approaches.

Here, they are split for the dense and dilute part of the spray using an indicator function Ψ which is equal to one if the liquid mass fraction, $\tilde{Y_l}$ is between 1 and 0.5 and is zero for cells with a liquid mass fraction less than 0.1. The indicator function can be written as a function of the liquid volume fraction, ϕ_l, where $\phi_l = \bar{\rho}\tilde{Y_l}/\bar{\rho_l}$ as,

$$\Psi(\phi_l) = H(\phi_l - 0.1)H(\phi_l - 0.5) + (H(\phi_l - 0.1) - H(\phi_l - 0.5))(2.5\phi_l - 0.25) \quad (19)$$

where $H()$ is the Heaviside step function. In an analogy of the Σ-equation of Vallet and Borghi (1999) a primer approximation for the terms on the RHS is to write them in the form

$$S = \frac{\bar{\Sigma}}{\tau_\Sigma}\left(1 - \frac{\bar{\Sigma}}{\bar{\Sigma}_{eq}}\right) \quad (20)$$

where $\bar{\Sigma}_{eq}, \tau_\Sigma$ are an equilibrium value for the interface and the time-scale of the corresponding process. A shortcoming of this restoration equilibrium model is that it is not well defined when no perturbations are present since at rest $\bar{\Sigma}_{eq} = 0$ which implies that for a finite time-scale τ_Σ the surface will be destroyed infinitely fast. The term S_{init} corresponds to the minimum liquid-gas surface produced in the atomisation process and is larger where the gradient of liquid mass fraction is higher. By the definition of $\bar{\Sigma}$, this minimum interface has to be proportional to the inverse of the integration kernel which can be also associated to the characteristic turbulent spatial scales. Following Menard et al. (2006) and assuming that the first blobs that form will be approximately of the scale of l_t, it is $S_{init} = Y_l(1 - Y_l)/l_t$ with the limiting case where liquid mass fraction becomes small where the minimum production of interface is a function of the liquid mass fraction gradient, $S_{init} = 2\frac{\mu_t}{Sc_t}\frac{6\bar{\rho}}{\rho_l \rho_g l_t}\frac{\partial \tilde{Y_l}}{\partial x_i}\frac{\partial \tilde{Y_l}}{\partial x_i}$. S_{turb} is the term responsible for the production or destruction of the interface density due to stretching caused by turbulence and collisions/coalescences in the dense part of the spray and is calculated using a formulation similar to Eq.20. It is assumed that interface will be created or destroyed due to turbulence until Σ reaches an equilibrium value, Σ^*_{turb} which is defined from an equilibrium Weber number We^*, $We^* = \rho_l \phi_l k/\sigma\Sigma^*_{turb}$ which is set to be equal to 1.0. The

turbulent time-scale τ_t for this process, in case of Reynolds-Averaged-Navier-Stokes (RANS), is equal to k/ϵ for the k-ϵ turbulence models and for the k-ω models it is $\tau_t = 1/\omega$, where k, ϵ, ω are the turbulent kinetic energy, turbulent kinetic energy dissipation and the specific turbulence dissipation respectively. In Large-Eddy-Simulations (LES) the turbulent time-scale is $\tau_t = ||S_{ij}||^{-1}$, where S_{ij} is the strain rate tensor. The source terms S_{coll} and S_{2nBU} for the surface creation/destruction due to collisions and the surface production due to secondary break-up in the dilute spray region are updated using the restoration equilibrium equation with different time-scales, $\tau_{coll}, \tau_{2ndBU}$ respectively. The equilibrium time-scales for S_{coll} is $\tau_{coll} = 1/\bar{\Sigma}\sqrt{2k/3}$ and the equilibrium Σ^*_{coll} for the collision-coalesence source term is calculated according to Lebas et al. (2009). The equilibrium timescale for S_{2nBU} is done using the experimental work of Pilch and Erdman (1987) in case of the secondary break-up and the equilibrium Σ^*_{2ndBU} is calculated for a Weber number equal to 12 at the limit of Ohnesorge number equal to zero (Pilch and Erdman, 1987; Lebas et al., 2009). More details for the source terms $S_{init}, S_{turb}, S_{coll}$ and S_{2nBU} are provided from Lebas et al. (2009).

3.2. Superheated jets

Finally, the last term in Eq.(18) are $S_{vap,den}, S_{vap,dil}$, which are responsible for the change in interface density due to evaporation. These terms are usually omitted in the literature since there is no available model valid for all the spray regions. In cryogenic superheated liquids such as R134A, evaporation could be important and can be influenced by mechanical effects. The distinction to dense and dilute contribution for the evaporation source term is proposed here for the first time since different conditions for the dense and dilute regions are acknowledged (Faeth, 2002). Accepting the classical view, drop evaporation dominates dilute sprays in the same way break-up dominates dense sprays. Hence, $S_{vap,dil}$ might have a contribution to the equation for Σ comparable to the other terms on the RHS of Eq.(18). In the dilute region, the liquid structures that occur in the flow can be considered to be spherical droplets.

Then it is

$$S_{vap,dil} = f_{v,s}\frac{\bar{\Sigma}^2}{\rho} \tag{21}$$

The logic behind this formulation is that the term $f_{v,s}$ is the mass transfer due to vaporisation per surface and is multiplied with the surface per area and surface per volume. The mass flux at the surface of a droplet of radius r_s is $f_{v,s} = m_v/4\pi r_s^2$, where m_v is the mass vaporisation rate typically taken from a droplet evaporation model. From Abramzon and Sirignano (1989) one gets $m_v = 2\pi\rho_g D_{32}\mathfrak{D}ln(1+B_M)Sh^*$, where $B_M = Y_l/(1-Y_l)$ is the mass transfer number (Spalding number). The modified Sherwood number, Sh^* depends on the flow characteristics, $Sh^* = Sh^*(Re, Sc)$ and is a function of Sherwood, Reynolds and Schmidt numbers. The modified Sh^* is calculated as in Abramzon and Sirignano (1989). Substituting the expression of D_{32} one gets

$$S_{vap,dil} = -\frac{\mathfrak{D}Sh^* ln(1+B_M)}{6Y_l}\left(\frac{\rho_l\rho_g}{\rho^2}\right)\bar{\Sigma}^3 \tag{22}$$

The above expression has units $[1/ms]$. It is important to mention that this formulation depends on the drop evaporation model expression that is used in each case. Ignoring the vapour film around the droplet, we can assume $Sh = Sh^*$ and the vaporisation model of Spalding (1953) can be retrieved. In the dilute region of the spray, we expect that evaporation on the drop surface leads to surface reduction alongside with the droplet radius decrease justified by the D^2-law. Consequently, a minus sign is included on the RHS of the above formula. The terms containing Y_l in Eq. 22 form a function of Y_l that tends to 1 for $Y_l \to 0$ and the source term scales to $K\Sigma^3$, where $K = \mathfrak{D}Sh^*/6$. Regarding the dense part, $S_{vap,den}$, a simple correlation is introduced here, originally proposed in Lyras et al. (2017),

$$S_{vap,den} = \frac{\bar{\Sigma}}{\Theta}\left(\frac{x_{eq}\rho_{eq}}{\rho} - x\right) \tag{23}$$

where the ρ_{eq} is the density at the thermodynamic equilibrium. Since in the primary atomisation region the liquid core is likely to remain in a metastable condition it is postulated that the relaxation time-scale might be appropriate in Eq.23. The time-scale Θ can be used regardless the boiling mechanism one

might assume for the numerical simulation, e.g. homogeneous or surface boiling. The evaporation source term contribution in the surface density equation is then summarised as

$$S_{vap} = \Psi \left[\frac{\bar{\Sigma}}{\Theta} \left(\frac{x_{eq}\rho_{eq}}{\rho} - x \right) \right] + (1-\Psi) \left[-\frac{Kln(1+B_M)}{Y_l} \left(\frac{\rho_l \rho_g}{\rho^2} \right) \bar{\Sigma}^3 \right] \quad (24)$$

The Σ-equation can now be written in its full form as

$$\frac{\partial \bar{\Sigma}}{\partial t} + \frac{\partial \tilde{u_j} \bar{\Sigma}}{\partial x_j} = \frac{\partial}{\partial x_j} \left(\frac{\nu_t}{Sc_t} \frac{\partial \bar{\Sigma}}{\partial x_j} \right) + \Psi \left[\frac{Y_l(1-Y_l)}{l_t} + \frac{\bar{\Sigma}}{\tau_t} \left(1 - \frac{\bar{\Sigma}}{\bar{\Sigma}^*_{turb}} \right) + \frac{\bar{\Sigma}}{\Theta} \left(\frac{x_{eq}\rho_{eq}}{\rho} - x \right) \right]$$
$$+ (1-\Psi) \left[\frac{\bar{\Sigma}}{\tau_{coll}} \left(1 - \frac{\bar{\Sigma}}{\bar{\Sigma}^*_{coll}} \right) + \frac{\bar{\Sigma}}{\tau_{2ndBU}} \left(1 - \frac{\bar{\Sigma}}{\bar{\Sigma}^*_{2ndBU}} \right) - \frac{Kln(1+B_M)}{Y_l} \left(\frac{\rho_l \rho_g}{\rho^2} \right) \bar{\Sigma}^3 \right] \quad (25)$$

The developed method is implemented within the open source CFD code OpenFOAM (Weller et al., 1998). Typically a second order bounded scheme is used to solve this equation together with a van Leer limiter. The method presented in the previous chapter for calculating the pressure is naturally coupled with the modified version of ELSA model proposed here. The vapour mass fraction equation is solved prior to the surface density equation calculating the mass fractions and the related source terms in Eq.(18). The HRM and modified ELSA are coupled for the first time with interface tracking to simulate superheated liquid jet atomisation. The PIMPLE algorithm, combination of the PISO and SIMPLE algorithms, (Ferziger and Peric, 2001) is used to couple pressure and velocity in a segregated manner. After calculating x with Eq.(1) the matrix $H(u_j)$ which contains all the terms the momentum equation, except for the gradient of pressure, is updated and is used to calculate the fluxes without the contribution of ∇p. The pressure equation is solved including the contributions of surface tension, thermal non-equilibrium e.t.c. and a new velocity field is obtained which will be relaxed (under-relaxation factors for pressure, velocity and surface density were within the range of 0.3 to 0.7). In most of the simulations 5 to 8 PISO loops were used with 1 to 3 outer loops for updating the $H(u_j)$ matrix using Courant numbers up to 2.2. Fixed values for pressure and velocity were imposed at the inlet flow with a boundary condition developed by Poinsot and Lelef (1992) for p and zero gradient for u at the low-pressure farfield (two-phase

jet outlet). For LES velocity and viscosity boundary conditions are set following Montorfano et al. (2013). A second-order bounded scheme (Jasak et al., 1999) for the convective terms was used for the calculations. The scheme is a blend of upwind and central scheme using a smooth transition between the low order to the second order scheme offering a good trade-off of accuracy and stability. Second order schemes with a linear correction were used for the gradient terms. The variables are stored in the cell centres in a co-located arrangement and they are interpolated at the cell faces.

4. Results and discussion

Results from numerical simulations regarding flashing R134A (1,1,1,2 – Tetrafluoroethane: $CF_3 - CH_2F$) are presented first. The experimental domain consists of a high-pressure region where R134A is stored at a pressure above its vapour pressure at ambient conditions (663 kPa at 293.15 K). The liquid passes through a nozzle of diameter D and length L and is released into a low-pressure region which is equal to the atmospheric pressure.

4.1. R134A jets: Zhou et al. (2012) experiment

Previous experimental studies describe that flashing might start either inside or outside the channel it emerges from, depending on the channel geometry and superheat conditions. Yildiz (2005) observed that for small L/D the axial velocity does not change in the vicinity of the nozzle exit. The reported large values of droplet Sauter mean diameter (SMD) might be an indication that the jet flashed outside the nozzle. On the other hand, internal flashing with forming bubble nuclei might lead to more catastrophic flow patterns that influence the jet dynamics. It is of major importance to investigate these changes in the spray patterns with respect to macroscopic changes. For this reason, the experimental work of Zhou et al. (2012) is studied here. In this experiment, R134A flows through a long nozzle with $L/D = 78.4$ and diameter equal to $D = 0.81mm$. The domain used for simulations is shown in Fig. 1. This test case is used here

to check grid dependence of the solution. We are interested to see if the pressure equation that updates p is sensitive to the computational mesh that is used for the solution. Different meshes were used with 1.0, 1.5 and 2.0 million cells for RANS calculations and the predicted pressure inside the nozzle is shown in Fig. 2. The coarse and the medium size meshes are very close to the fine mesh results through the nozzle length with a small difference at the inlet of the nozzle. The local minimum of the pressure is also observed in previous studies Park et al. (1997); Schmidt et al. (2010); Lyras et al. (2018).After a smooth profile through the nozzle, the pressure drops upstream the nozzle exit due to the rapid phase change that occurs. In Figs. 3- 4 the predicted liquid volume fraction and the mean surface density along the jet axis downstream the nozzle exit are plotted. The results are normalised with the maximum value along the centreline. As the expected the liquid volume fraction is maximum at the nozzle exit and gradually decreases moving further downstream where the impact of flash-boiling and aerodynamic break-up become more evident. The $\bar{\Sigma}$ appears to increase downstream the nozzle exit, and after reaching a maximum decreases at the dilute region of the jet. Increasing the mesh resolution is expected to decrease the calculated mean surface density in the ELSA method as the volume that $\bar{\Sigma}$ is integrated is smaller. The maximum point follows similar trend as the one observed in the experiment for the droplet number density. Similar behaviour is also observed in previous studies (Lebas et al., 2009; Navarro-Martinez, 2014). Next, the results from the medium mesh are shown. The spray characteristics, the velocity and the Sauter mean diameter at various positions were measured. The flow patterns inside the nozzle were not studied in the experiment. Both RANS and LES framework were used. In Fig. 5 an example of small-scale LES simulations is shown for the experiment. The iso-contours of $\tilde{Y}_l = 0.28$ are included to illustrate the very first stages of the liquid jet atomisation. The outlet patches of the simulated domain were far enough, typically in more than $50D$ distance from the jet axis in the radial direction, and at $193D$ from the nozzle exit. RANS results are presented here for validation. The results were taken until steady state reached and any boundary

effect at the far-field, downstream the nozzle has negligible impact. All the physical parameters of the experiment are listed in Table 1. The axial velocity profiles are shown in Fig. 6 as a function of the radial distance at two different positions. The axial velocity takes its maximum at the jet centreline in all cases. This is in accordance to the experimental and theoretical studies (Abramovich, 1963). An obvious differentiation occurs for the rate of the velocity decrease moving towards the jet periphery. The results indicate that the distance from the nozzle exit plays a role in the jet dispersion. Axial velocity decreases faster closer to the release point $x = 50mm$ ($x/D = 61.7$), compared to the position $x = 90mm$ ($x/D = 111$) where velocity changes in a smoother manner. This smaller gradient in the largest distance results indicates a more uniform jet morphology in the droplet cloud. The maximum predicted axial velocity at the $x = 50mm$ position is around 35 m/s. The spray velocity starts to increase fast (in the so-called expansion zone) and becomes maximum and then decreases again (entrainment zone). The maximum at the numerical results occurs at approximately x=60mm ($x/D = 60$) whereas in experiments the peak value was observed for a small number of particles in x=40mm ($x/D = 49$). This increase in the axial velocity of the spray was not observed in Allen (1998) and a small increase in Yildiz (2005) was reported. The axial velocity is shown in Fig. 7. The jet, after emerging at the low-pressure region, is a dense spray consisting of droplets moving through a vapour cloud, which is a direct consequence of the evaporation mechanism. The acceleration of the droplets is attributed by the authors of the experiment, to the explosive character of the atomisation of the cryogen. Up to the maximum velocity point, the liquid core might be considered to be practically intact. The velocity starts to decrease due to drag forces which prevail over the inertia forces and govern the droplets' kinematics. From a numerical point of view, this acceleration imposes some major challenges in terms of stability and an under-relaxation procedure is recommended. The rapid increase and decrease in the axial velocity might cause weakness to the pressure-velocity coupling, and a good choice of turbulence model from the k-ω family with near-wall treatment is required. Here the SST-$k - \omega$ model of

Menter (1993) is employed.

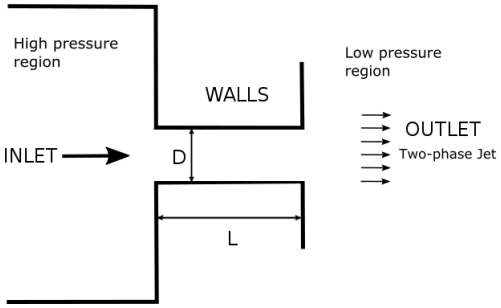

Figure 1: Schematic of the domain used in simulations. The superheated liquid flows through the channel and exits at the low-pressure region as a two-phase jet.

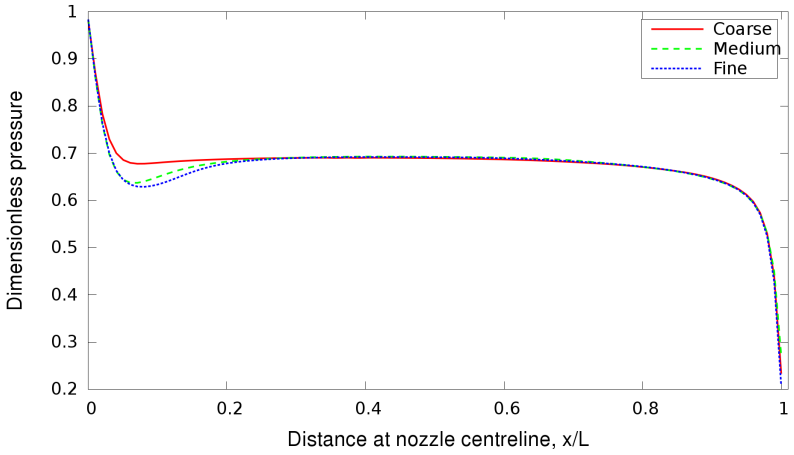

Figure 2: Predicted pressure distribution along the nozzle for different meshes for flashing R134A Zhou et al. (2012) experiment.

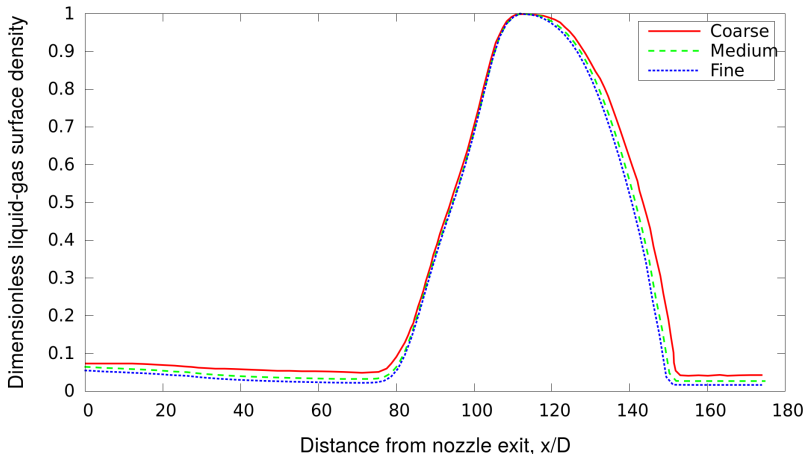

Figure 3: Predicted normalised mean surface density along the jet axis for different meshes for flashing R134A Zhou et al. (2012) experiment.

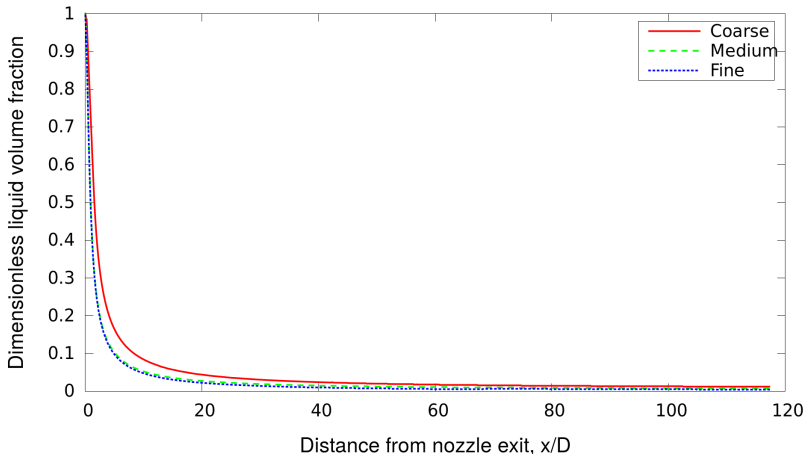

Figure 4: Predicted normalised liquid volume fraction along the jet axis for different meshes for flashing R134A Zhou et al. (2012) experiment.

Regarding the spatial scale of the liquid structures, results for the D_{32} are shown in Fig. 8. Quantifying the size of ligaments and blobs that form within the jet is not a trivial task. The limited visibility of the moving particles and the need for non-intrusive measurement techniques makes the experimental charac-

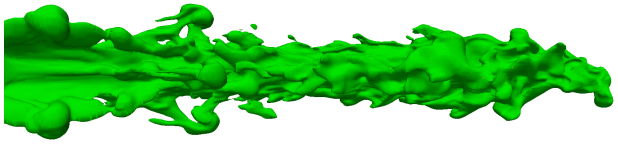

Figure 5: Snapshot of iso-contour $\tilde{Y}_l$ for LES simulations at the first 5mm of spray motion downstream the nozzle exit. A mean cell size equal to $4\mu m$ was used close to the nozzle exit.

Table 1: Physical properties for simulations.

	Physical parameters for simulations
Inlet pressure	700 kPa
Inlet temperature	247 K
Outlet pressure	100 kPa
Outlet temperature	298 K
L/D	78.4
Nozzle diameter	0.81mm
Thermodynamic conditions	Saturated

terisation of the mean droplet size extremely difficult. Statistical analysis of the Phase Doppler Particle Analyzer (PDPA) results gave the SMD which is used for comparison here. Fig. 8 shows the radial variations of SMD for $x/D = 61.7$ and $x/D = 111$. The model overestimated the D_{32} closer to the jet centreline and showed good agreement after $1.5D$ distance in the radial direction. This behaviour is reasonable and appears in other numerical studies (Vallet et al., 2001). This can be caused due to the numerical parameters used in the Σ-equation and the source terms in particular. The equilibrium values are also subject to numerical tuning. The difference might also be an indication for changing the HRM constants for R134A. The HRM contribution is both in the pressure update and equation Eq.(18). A slightly increasing trend in the D_{32} observed in the experiments is also captured from the atomisation model. Fig. 8 illustrates the multi-scale character of flash-boiling atomisation. The nozzle length of the

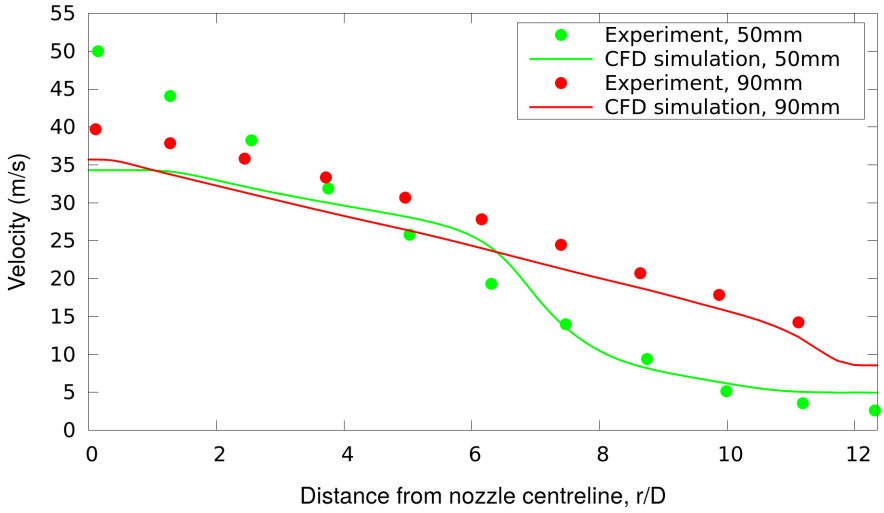

Figure 6: Radial velocity at x=50, 90mm. Comparison with Zhou et al. (2012).

experiment was $L = 63mm$. Moving along the nozzle, the flashing inception begins in the internal flow, and one might reasonably assume that at some point the regime transition from pure liquid to a dispersed flow happens. The size of the droplets can be comparable to the nozzle diameter, $O(10^{-3})m$ initially, and drops due to mechanical and thermodynamic effects becoming $O(10^{-6})m$ at the measured axial positions and at the radial direction. Hence, the average particle size can be reduced to one thousand times its original size.

The reason for this reduction in spatial scale of the blobs and droplets can be attributed to the explosive character of the atomisation. This character is fundamentally associated with the flashing mechanism which starts inside the nozzle. Results in Fig. 8 for D_{32} simulating the same experiment but without considering the internal flow reveal a higher deviation with experiments at $x = 50mm$ but smaller in the $x = 90mm$ position. Exclusion of the internal flow simulation tends to under-predict the SMD at $r/D = 3$ and afterwards for both positions. The droplets emerge to the atmosphere at a temperature higher than the saturation temperature and become locally superheated. This metastable

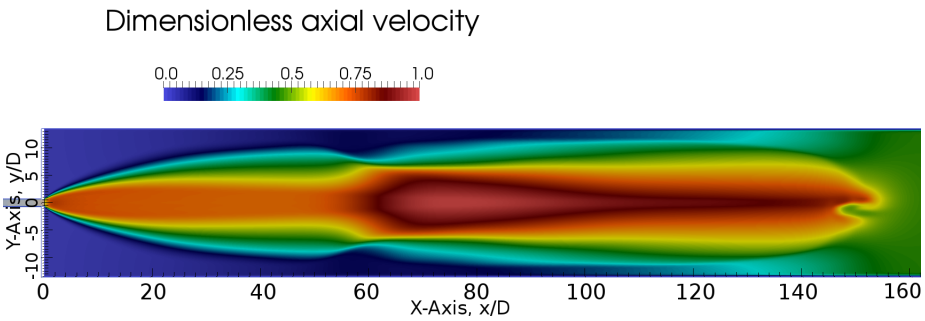

Figure 7: Distribution of dimensionless axial velocity u_x/u_{max} along the distance x/D.

state follows a violent liquid fragmentation (explosive atomisation) with new smaller droplets. Moving further away from the nozzle exit, the flow is expected to become more uniform, with droplet evaporation becoming more important. Droplet evaporation manifests that the smaller droplets moving at the periphery of the jet become smaller until they are practically negligible. Under these conditions, the mean surface density decreases (Fig. 9) which means that

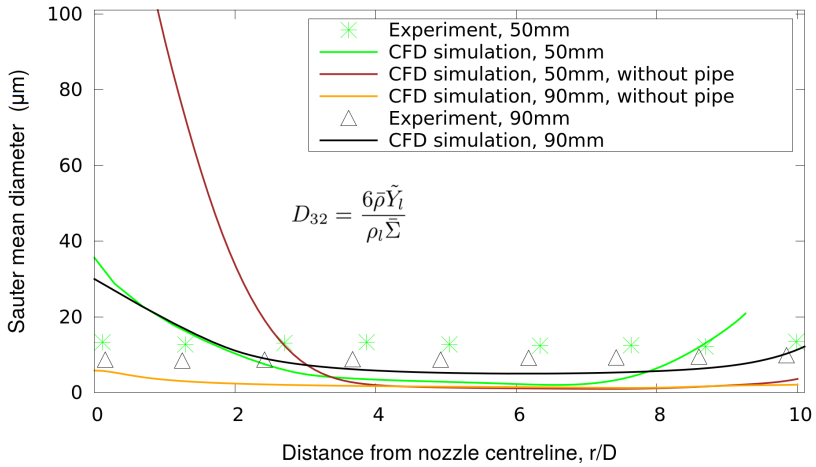

Figure 8: Sauter mean diameter (SMD) at x=50, 90mm. Comparison with Zhou et al. (2012).

the SMD becomes bigger ($D_{32} \propto 1/\bar{\Sigma}$), hence the increasing trend in Fig. 8.

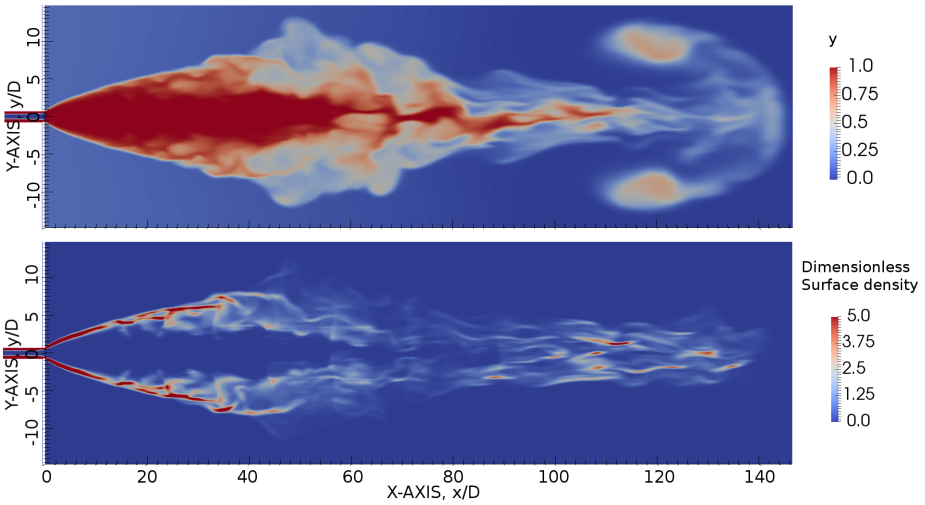

Figure 9: Distribution of dimensionless liquid and vapour mass fraction, y and surface density, Σ/Σ_0 along the jet centreline.

In Fig. 9 the surface density is shown normalised with a theoretical initial value $\Sigma_0 = 1/\Delta^3$ where Δ is the LES filter used in the simulations. This is the value that Σ will scale with a very fine mesh, Navarro-Martinez (2014). This value is expected to be the upper limit for Σ in dilute regions where only small blobs and droplets exist (sub-grid scale). Comparing the results in D_{32} with the experimental findings of Yildiz (2005) one might elucidate the impact of the nozzle length-to-orifice ratio on the spray dynamics. The average D_{32} in the experiment considered here ($L/D = 78.4$) for a long nozzle was less than $15\mu m$ whereas for an inlet pressure approximately 8bar and a short nozzle with $L/D = 2$ the measured average droplet sizes were much higher and remained always greater than $50\mu m$. The nature of the relationship between L/D and SMD was studied by Yildiz (2005). In particular, at $x/D = 110$ the higher values of D_{32} for the longer nozzle were justified from the incomplete atomisation that occurred inside the nozzle for the case of nozzles with larger L/D. Nevertheless, the L/D used in Zhou et al. (2012) was much larger, and the internal flashing

is expected to cause bubble nucleation and bursting earlier, giving in general smaller droplet sizes. A three-dimensional caption of the liquid jet atomisation for shorter $L/D = 4$ using LES and a mesh with 15 million cells is presented in Fig. 10.

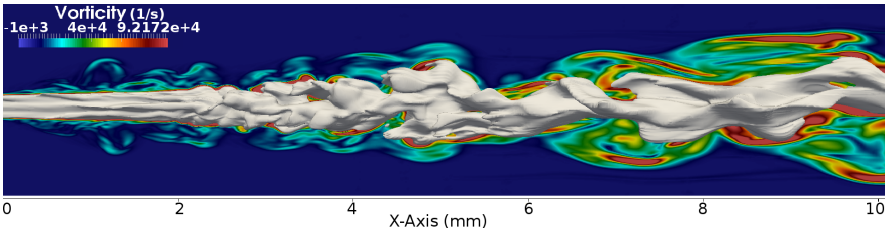

Figure 10: Iso-contour for y=0.47 with the magnitude of vorticity using LES for the first 10mm of the spray. The physical parameters are the same as in Zhou et al. (2012) but for shorter nozzle $L/D = 4$.

4.2. Water experiments: Park and Lee (1994)

The next flashing scenario examined is for water jets flowing through sharp nozzles. The classic experiments of Park and Lee (1994) are considered here. The test cases were for small pressures up to 4bar and initial temperatures up to 125^oC. A long nozzle was used which offers an opportunity to study the internal flashing mechanism in a domain similar to the one in Fig. 1. All the major physical properties for the simulations are listed in Table 2. LES was tested for simulating the internal flow and the primary atomisation region up to a distance 7D from the nozzle exit using a computational mesh with 17 million hexahedral cells. The smallest grid cells for this simulation are 10μm in x (axial direction) with 5μm cells in y and z. The D_{32} in the spray downstream the nozzle exit in the experiments was observed to be more than 100μm (low-pressure regime) allowing for a grid size Δx to be $\Delta x > 10D_{32}$. A Gaussian filter Δ was used for the simulations. For the developed turbulent length scale L_t in the present LES, comperable to the nozzle diameter (Pope, 2000; Hamad and Ganesan, 2015), it is expected to have a ratio L_t/Δ not less than one (Pope, 2000).

The Smagorinsky model was used and the sub-grid-scale Reynolds stress, τ^{sgs} is modelled as $\tau_{ij}^{sgs} - 1/3\tau_{kk}^{sgs}\delta_{ij} = 2\mu_t\bar{S}_{ij}$. The sub-grid-scale eddy viscosity can be derived by dimensional arguments to be equal to $\mu_t = C_S^2\rho\Delta^2 \parallel \bar{S} \parallel$, where $\parallel \bar{S} \parallel = (\bar{S}_{ij}\bar{S}_{ij})^{1/2}$. Here, a low value of the constant $C_S = 0.065$ is used, recommended for channel flows. Results shown in Fig. 11 for the liquid-gas interface show the gradual liquid fragmentation though time. The long channel and the low inlet pressure resulted in an increased residence giving time for bubbles to form, burst and collapse signalling a regime change. The growing waves acting on the jet start to influence the jet and the result of these perturbations is evident after some reasonable time, which is expected according to Rayleigh's theory (is more clear here after t=0.0006s). Moving further downstream the nozzle exit, the liquid surface decreases due to large ligaments and blobs shedding to smaller structures. The authors of the experiment investigated a thorough analysis for determining primarily the relationship between the superheat degree and the spray characteristics in low pressure flashing jets. In their study they concluded that for long nozzles bubble nucleation starts at the walls region. They distinguished three regimes for the internal flow: bubbly, annular and slug. They observed that for low superheat degrees the bubbly regime is sustained across the nozzle with bubble formation and growth moving towards the nozzle exit. The bubbles burst outside the nozzle fragmenting the liquid core into ligaments. The intact liquid core becomes shorter with increasing the superheat degree. In this case the bubble nucleation inside the nozzle was reported to be more extensive, predicating a slug or annular regime for the channel flow. During the primary atomisation process in slug regime, the slug bubbles that form from smaller bubbles that collide and coalesce, burst into ligaments. On the other hand, in the annular regime the liquid phase was moved towards the walls and then an enhanced disintegration downstream the nozzle exit due to the interactions with the vapour core gave generally smaller SMD values for the droplets. RANS results for a mesh of 200,000 cells are shown in Fig. 12. Both coarser (100,000 cells) and finer (300,000 cells) meshes were used. The numerical results in Fig. 12 seem to agree with the observations of Park

and Lee (1994) that increasing the degree of superheat, the SMD decreases, at least for a constant pressure. Fig. 12 illustrates the mean SMD value at the radial direction at distance $x = 50mm$ (x/D=33.3). Results are plotted using the normalised superheat degree $\Delta\check{T}_{sh}$ with respect to the ambient conditions (out)

$$\Delta\check{T}_{sh} = \frac{T_{in} - T_{sat}(p_{out})}{T_{sat}(p_{in}) - T_{sat}(p_{out})} \tag{26}$$

Small values of $\Delta\check{T}_{sh}$ indicate a non-superheated state of the liquid jet and for $\Delta\check{T}_{sh} = 1$ the liquid boils inside the storage vessel. The results show good agreement for higher superheat degrees. The deviation for $\Delta\check{T}_{sh} = 0.2$ could be associated to the higher residence time inside the channel and the Σ-equation constants. The impact of the initial storage pressure is illustrated in the experimental and numerical results. Bubble nucleation appears to attain a random occurrence pattern. Pressure change might also alter the jet stability, with higher pressures leading to a more stable regime (Wang et al., 2017). For the same pressure (p=3bar) increasing $\Delta\check{T}_{sh}$ reduces the SMD. This could be connected to the number of bubbles inside the nozzle which is expected to increase with increasing the superheat degree since the surface tension of the vapour decreases with a consequent decreasing for the departure diameter for the bubble (Hutcherson et al., 1983). Hence, the internal flow becomes more bubbly. In the numerical results, the mean SMD reduces approximately 43 percent of the value for $\Delta\check{T}_{sh} = 0.3$ and in the experiments the mean Sauter mean diameter is 33 percent of the former. On the contrary, keeping the temperature constant, $T_{in} = 110^oC$ and decreasing the pressure from 4bar ($\Delta\check{T}_{sh} = 0.2$) to 3bar ($\Delta\check{T}_{sh} = 0.5$) the mean D_{32} decreased approximately $20\mu m$ in the experiment but slightly increases a few microns in the CFD results. The effect of the pressure on the droplet SMD was also studied by Cleary (2008) who suggested that $D_{32} \propto p^{-0.54}$. This suggests that increasing the pressure D_{32} decreases, at least within the limits of the proposed correlation ($L/D < 50$). Fig. 13 shows the dimensionless spray angle which is the calculated spray angle divided by its maximum value. Both in experiments and CFD the angle is defined as the

Table 2: Physical properties for simulations.

	Physical parameters for simulations
Inlet pressure	20-40 kPa
Inlet temperature	110-125^oC
Outlet pressure	100 kPa
Outlet temperature	25^oC
L/D	72
Nozzle diameter	1.5mm
Thermodynamic state	Saturated

included angle between the lines connecting the nozzle exit and the points at the spray edge at 20mm (x/D=13.3) downstream the nozzle exit. The angle shows initially an increasing trend increasing the superheat for both cases of 2bar and 3bar. Higher values of superheat correspond to an increment in the number of critical vapour nuclei that form per unit volume and time, J. For higher temperatures, the waiting time for the critical nuclei to form decreases ($\tau \sim 1/J$) giving rise in nucleation rate (Avedisian, 1985) and consequently more vapour appears in jet (see Fig. 14). The jet dispersion in the radial direction is wider which indicates that the spray angle is larger. As Park and Lee (1994) point out, the bubbles that form burst and increase the velocity in the radial direction. The spray angle increases until it reaches a maximum and decreases rapidly after. The maximum angle location is not the same for each case. For inlet pressure equal to 2bar it occurs at approximately in $\check{\Delta T}_{sh} \simeq 0.9$ ($T_{in} = 122.5^oC$) whereas for the case of 3bar, it occurs at approximately in $\check{\Delta T}_{sh} \simeq 0.65$ ($T_{in} = 120^oC$). The spray angle after reaching its maximum starts to decrease due to entrainment effects (see Fig. 15). The enhanced atomisation results in a finer spray and the smaller droplets, which are influenced more by drag forces, vaporise until they become negligible.

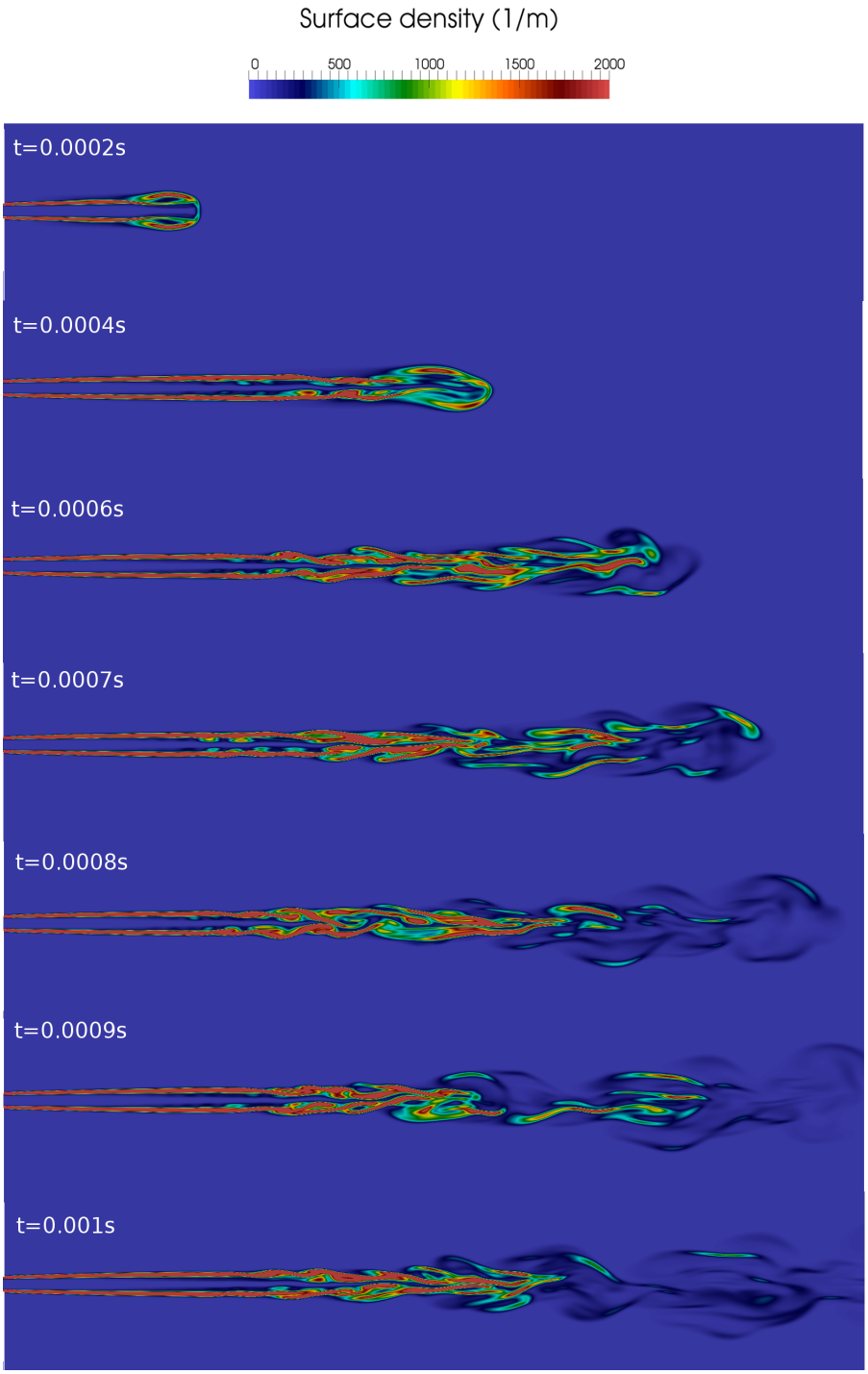

Figure 11: Evolution of Σ with respect to time from 3D LES for flashing water up to 7D distance from the jet exit.

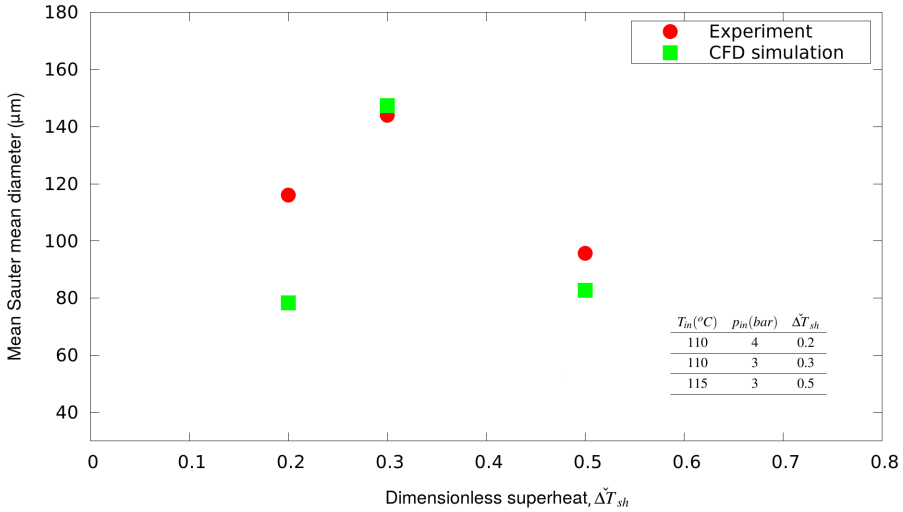

Figure 12: Cross-sectional averaged SMD versus the dimensionless superheat $\Delta\check{T}_{sh}$ at 50mm (x/D=33.3) distance downstream the nozzle exit. Comparison with Park and Lee (1994).

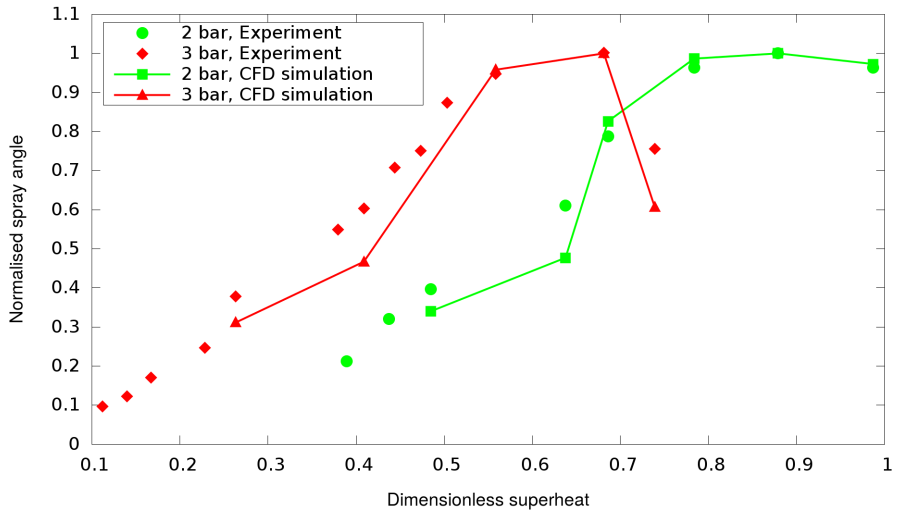

Figure 13: Normalised spray angle with respect to the dimensionless superheat $\Delta\check{T}_{sh}$ at 50mm (x/D=33.3) distance downstream the nozzle exit. Comparison with Park and Lee (1994).

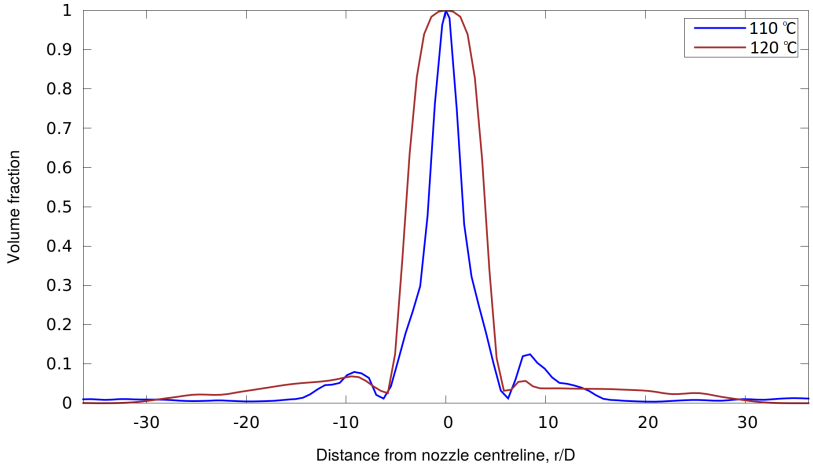

Figure 14: Liquid volume fraction at the radial direction for two different initial temperatures at x=20mm.

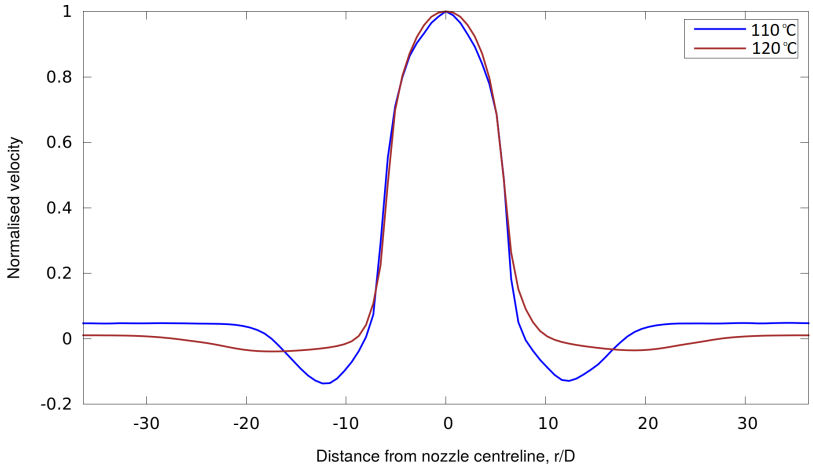

Figure 15: Velocity profile at the radial direction, u_x/u_{max} for two different initial temperatures at x=20mm.

5. Conclusion

A novel method for modelling the atomisation of flashing jets is presented in this paper. The method is coupled with a newly developed pressure equa-

tion for flash boiling constructing a unified approach for modelling superheated jets primary atomisation and secondary break-up considering the flow inside the channel they emerge from. This is an Eulerian approach for modelling the spray motion and employs the liquid-gas interface density concept. Based on the existing ELSA models, a new extension is proposed for the Σ-equation which is appropriate for the evaporation contribution in Σ in the dense and dilute spray regions. This new Σ-Y model has the capability to simulate all the stages of flashing jets atomisation. A validation series is presented for some important spray characteristics such as the Sauter mean diameter of the droplets, the velocity and spray angle. Different flashing jets scenarios are demonstrated for flashing water and R134A for validation and predictions for the droplet characterisation of superheated jets. The model can be easily implemented in pressure-based CFD codes for turbulent reactive flows allowing the description of the jet disintegration into liquid ligaments and droplets. The modified Σ equation employs constants for the surface creation and destruction from previous direct numerical simulations and experiments for specific liquids. This induces uncertainties especially for the evaporation source terms. Hence, parametric studies for model calibration for realistic flashing releases would give insights regarding the optimum selection of the numerical constants. Further research should be made for the implicit/explicit treatment of the source terms in the Σ-Y model and the impact of the turbulence modelling approach on the primary atomisation.

Acknowledgements

The authors would like to thank Prof. David P. Schmidt from the University of Massachusetts, Amherst and the Marie Curie Action of the 7th Framework Program of the European Union. The current work is part of the SafeLNG project (Project ID: 606754) regarding the numerical characterisation and simulation of the complex physics underpinning the Safe Handling of Liquefied Natural Gas (2014-2017).

References

Abramovich, G.N., 1963. The Theory of Turbulent Jets. Cambridge, Mass, M.I.T. Press.

Abramzon, B., Sirignano, W., 1989. Droplet vaporization model for spray combustion calculations. International Journal of Heat and Mass Transfer 32, 1605–1618.

Allen, J., 1998. Laser-based measurements in two-phase flashing propane jets. part one: velocity profiles1some aspects of the work described in this paper were presented at the ukala symposium on laser anemometry and computational solutions, university of loughborough, 2nd-3rd july, 1997.1. Journal of Loss Prevention in the Process Industries 11, 291–297. doi:https://doi.org/10.1016/S0950-4230(98)00015-1.

Aris, R., 1962. Vectors, Tensors and the Basic Equations of Fluid Mechanics. Prentice Hall Inc., Englewood Cliffs.

Avedisian, C.T., 1985. The homogeneous nucleation limits of liquids. Journal of Physical and Chemical Reference Data 14, 695–729. doi:10.1063/1.555734.

Benajes, J., Pastor, J., Payri, R., Plazas, A., 2004. Analysis of the influence of diesel nozzle geometry in the injection rate characteristic. Journal of Fluids Engineering 126, 63–71.

Bilicki, Z., Kestin, J., 1990. Physical aspects of the relaxation model in two-phase flow. The Royal Society 428, 379–397. doi:10.1098/rspa.1990.0040.

van den Bosch, C.J.H., Waterings, R., 2005. Methods for the calculation of physical effects. TNO yellow book, second edition.

Brackbill, J.U., Kothe, D.B., Zemach, C., 1992. A continuum method for modeling surface tension. J. Comput. Phys. 100, 335–354. doi:10.1016/0021-9991(92)90240-Y.

Cleary, V.M., 2008. Source Term Models for Superheated Releases of Hazardous Materials PhD thesis. University of Wales Cardiff, Cardiff.

Crowe, C.T., 2005. Multiphase Flow Handbook. Mechanical and Aerospace Engineering Series, CRC Press.

Delhaye, J., 1976. Sur les surfaces volumiques locale et inte grale en e coulement diphasique. C. R. Acad. Sci. Paris t. 282, 243–246.

Downar-Zapolski, P., Bilicki, Z., Bolle, L., Franco, J., 1996. The non-equilibrium relaxation model for one-dimensional flashing liquid flow. International Journal of Multiphase Flow 22, 473–483. doi:https://doi.org/10.1016/0301-9322(95)00078-X.

Duke, D., Battistoni, M., Swantek, A., Sovis, N., Kastengren, A., Powell, C., Som, S., Schmidt, D., 2015. Validation of cavitation simulations in submerged nozzles. ILASS .

Edelbauer, W., 2017. Numerical simulation of cavitating injector flow and liquid spray break-up by combination of eulerianeulerian and volume-of-fluid methods. Computers & Fluids 144, 19–33. doi:https://doi.org/10.1016/j.compfluid.2016.11.019.

Faeth, G., 2002. Dynamics of secondary drop breakup-a rate controlling process in dense sprays. Proceedings of the ILASS-Europe 2002 .

Ferziger, J., Peric, M., 2001. Computational Methods for Fluid Dynamics. Springer Berlin Heidelberg.

Hamad, F., Ganesan, P., 2015. Effect of drops on turbulence of kerosenewater two-phase flow in vertical pipe. International Journal of Heat and Fluid Flow 56, 152 – 159. doi:https://doi.org/10.1016/j.ijheatfluidflow.2015.07.020.

Hervieu, E., Veneau, T., 1996. Experimental determination of the droplet size and velocity distributions at the exit of the bottom discharge pipe of a liquefied propane storage tank during a sudden blowdown. Journal of Loss

Prevention in the Process Industries 9, 413–425. doi:https://doi.org/10.1016/S0950-4230(96)00030-7.

Hutcherson, M.N., Henry, R.E., Wollersheim, D.E., 1983. Two-phase vessel blowdown of an initially saturated liquidpart 2: Analytical. ASME. J. Heat Transfer. 105, 694–699.

Ishii, M., 1975. Thermo-fluid Dynamic Theory of Two-phase Flow. Eyrolles. Paris/Scientific and Medical Publications of France, New York.

Ishimoto, J., Ohira, K., Okabayashi, K., Chitose, K., 2008. Integrated numerical prediction of atomization process of liquid hydrogen jet. Cryogenics 48, 238–247. doi:https://doi.org/10.1016/j.cryogenics.2008.03.006.

Jasak, H., 1996. Error Analysis and Estimation for the Finite Volume Method with Applications to Fluid Flows PhD thesis. Ph.D. thesis. Imperial College.

Jasak, H., Weller, H.G., A. D., G., 1999. High resolution nvd differencing scheme for arbitrarily unstructured meshes. International Journal for Numerical Methods in Fluids 31, 431–449. doi:10.1002/(SICI)1097-0363(19990930)31:2<431::AID-FLD884>3.0.CO;2-T.

Jiang, X., Siamas, G., Jagus, K., Karayiannis, T., 2010. Physical modelling and advanced simulations of gasliquid two-phase jet flows in atomization and sprays. Progress in Energy and Combustion Science 36, 131–167.

Johnson, D.W., Woodward, J.L., 1999. Release: a model with data to predict aerosol rainout in accidental releases. A CCPS concept book, American Institute of Chemical Engineers.

Kataoka, I., Ishii, M., Serizawa, A., 1986. Local formulation and measurements of interfacial area concentration in two-phase flow. International Journal of Multiphase Flow 12, 505–529. doi:https://doi.org/10.1016/0301-9322(86)90057-1.

Lebas, R., Menard, T., Beau, P., Berlemont, A., Demoulin, F., 2009. Numerical simulation of primary break-up and atomization: Dns and modelling study. International Journal of Multiphase Flow 35, 247–260. doi:https://doi.org/10.1016/j.ijmultiphaseflow.2008.11.005.

Lee, J., Madabhushi, R., Fotache, C., Gopalakrishnan, S., Schmidt, D., 2009. Flashing flow of superheated jet fuel. Proceedings of The Combustion Institute 32, 3215–3222.

Lhuillier, D., 2003. Dynamics of interfaces and rheology of immiscible liquidliquid mixtures. Comptes Rendus Mcanique 331, 113–118. doi:https://doi.org/10.1016/S1631-0721(02)00004-9.

Ling, Y., Zaleski, S., Scardovelli, R., 2015. Multiscale simulation of atomization with small droplets represented by a Lagrangian point-particle model. International Journal of Multiphase Flow 76, 122–143. doi:10.1016/j.ijmultiphaseflow.2015.07.002.

Lyras, K., Dembele, S., Schmidt, D., Wen, J., 2018. Numerical simulation of subcooled and superheated jets under thermodynamic non-equilibrium. International Journal of Multiphase Flow 102, 16–28.

Lyras, K., Dembele, S., Vendra, C.R., Wen, J., 2017. Numerical simulation of superheated jets using an eulerian method. ILASS-Europe 2017 .

Marle, C., 1982. On macroscopic equations governing multiphase flow with diffusion and chemical reactions in porous media. International Journal of Engineering Science 20, 643–662. doi:https://doi.org/10.1016/0020-7225(82)90118-5.

Menard, T., Beau, P.A., Tanguy, S., Demoulin, F.X., Berlemont, A., 2006. Primary break-up: Dns of liquid jet to improve atomization modelling. Computational Methods in Multiphase Flow III 50, 343–352.

Menter, F., 1993. Zonal two equation k- turbulence models for aerodynamic flows. AIAA Paper 93-2906 .

Montorfano, A., Piscaglia, F., Ferrari, G., 2013. Inlet boundary conditions for incompressible les: A comparative study. Mathematical and Computer Modelling 57, 1640–1647. doi:https://doi.org/10.1016/j.mcm.2011.10.077.

Morel, C., 2007. On the surface equations in two-phase flows and reacting single-phase flows. International Journal of Multiphase Flow 33, 1045–1073. doi:https://doi.org/10.1016/j.ijmultiphaseflow.2007.02.008.

Moulai, M., Grover, R., Parrish, S., Schmidt, D., 2015. Internal and near-nozzle flow in a multi-hole gasoline injector under flashing and non-flashing conditions, SAE International. doi:10.4271/2015-01-0944.

Navarro-Martinez, S., 2014. Large eddy simulation of spray atomization with a probability density function method. International Journal of Multiphase Flow 63, 11–22.

Oza, R.D., 1984. On mechanism of flashing injection of initially subcooled fuels. Journal of Fluid Mechanics 106, 105–109.

Park, B.S., Lee, S.Y., 1994. An experimental investigation of the flash atomization mechanism. Atomization and Sprays 4, 159–179.

Park, C.K., J. W. Park, M.K.C., Chung, M.H., 1997. An emperical correlation for the critical flow rates of subcooled water through short pipes with small diameters. Journal of the Korean Nuclear Society 29, 35–44.

Pavlov, P., 1988. Dynamics of Superheated Liquid Boiling. Sverdlovsk.

Pilch, M., Erdman, C., 1987. Use of breakup time data and velocity history data to predict the maximum size of stable fragments for acceleration-induced breakup of a liquid drop. International Journal of Multiphase Flow 13, 741–757. doi:https://doi.org/10.1016/0301-9322(87)90063-2.

Poinsot, T.J., Lelef, S.K., 1992. Boundary conditions for direct simulations of compressible viscous flows. Journal of Computational Physics 101, 104–129. doi:https://doi.org/10.1016/0021-9991(92)90046-2.

Pope, S.B., 2000. Turbulent Flows. Cambridge University Press. doi:10.1017/CBO9780511840531.

Price, C., Hamzehloo, A., Aleiferis, P., Richardson, D., 2016. An approach to modeling flash-boiling fuel sprays for direct-injection spark-ignition engines. Atomization and Sprays 26.

Prosperetti, A., Tryggvason, G., 2009. Computational Methods for Multiphase Flow. Cambridge University Press.

Reitz, R.D., 1990. A photographic study of flash-boiling atomization. Aerosol Science and Technology 12, 561–569. doi:10.1080/02786829008959370.

Schmidt, D.P., Gopalakrishnan, S., Jasak, H., 2010. Multi-dimensional simulation of thermal non-equilibrium channel flow. International Journal of Multiphase Flow 36, 284–292. URL: http://www.sciencedirect.com/science/article/pii/S030193220900192X, doi:https://doi.org/10.1016/j.ijmultiphaseflow.2009.11.012.

Sher, E., Bar-Kohany, T., Rashkovan, A., 2008. Flash-boiling atomization. Progress in Energy and Combustion Science 106, 417–439.

Spalding, D.B., 1953. The Combustion of Liquid Fuels. A Proc. 4th Symp. (Int.) on Combustion, Williams and Wilkins, Baltimore, MD.

Srinivasan, V., Salazar, A., Saito, K., 2010. Modeling the disintegration of cavitating turbulent liquid jets using a novel vof-cimd approach. Chemical Engineering Science 65, 2782–2796.

Tomar, G., Fuster, D., Zaleski, S., Popinet, S., 2010. Multiscale simulations of primary atomization. Computers & Fluids 39.

Vallet, A., Borghi, R., 1999. Modelisation eulerienne de iatomisation dun jet liquide. C. R. Acad. Sci. Paris, t. 327 t. 327, 1115–1200.

Vallet, A., Burluka, A., Borghi, R., 2001. Development of an eulerian model for the atomization of a liquid jet. Atomization and Sprays 11, 619–642.

Wang, X., Chen, B., Wang, R., Xin, H., Hui, Zhu, Z., 2017. Experimental study on the relation between internal flow and flashing spray characteristics of r134a using straight tube nozzles. International Journal of Heat and Mass Transfer 114, 675–687.

Weller, H.G., Tabor, G., Jasak, H., Fureby, C., 1998. A tensorial approach to computational continuum mechanics using object-oriented techniques. Comput. Phys. 12, 620–631. URL: http://dx.doi.org/10.1063/1.168744, doi:10.1063/1.168744.

Witlox, H.W.M., Bowen, P.J., 2002. Flashing liquid jets and two-phase dispersion A review. HSE.

Yildiz, D., 2005. Experimental investigation of supeheated liquid jet atomization due to flashing phenomena PhD thesis. von Karman institute, Universite libre De Bruxelles.

Zhou, Z.F., Wu, W., Chen, B., Wang, G.X., Guo, L., 2012. An experimental study on the spray and thermal characteristics of r134a two-phase flashing spray. International Journal of Heat and Mass Transfer 55, 4460–4468. doi:https://doi.org/10.1016/j.ijheatmasstransfer.2012.04.021.